UC Davis
UC Davis Previously Published Works

Title

Inertial Force Actuator Applications to Active Vehicle Suspensions

Permalink

Journal

2021 International Conference on Bond Graph Modeling and Simulation, ICBGM 2021(53(3))

ISSN

07359276

Author

McCrone, Jordan

Publication Date

2021-11-01

Peer reviewed

INERTIAL FORCE ACTUATOR APPLICATIONS TO ACTIVE VEHICLE SUSPENSIONS

Jordan McCrone
Donald L. Margolis
Department of Mechanical and Aerospace Engineering
University of California, Davis, USA.
djmccrone@ucdavis.edu, dlmargolis@ucdavis.edu

ABSTRACT

The application of inertial force actuators (IFAs) to vehicle dynamics is investigated. These are modeled as translational motors with a small proof mass attached at one end, such that forces applied by the actuator to the vehicle result in displacement of the proof mass in inertial space. IFAs would provide specific benefits compared to traditional active suspensions, which exhibit deleterious effects on secondary vehicle signals while pursuing their primary objectives. Since IFAs can be high power and generate high force magnitudes, and are constrained only by their internal stroke and force limits, their application is well suited for zero-mean band-limited white noise inputs such as a vehicle roadway. The suspension control problem is studied with the incorporation of IFAs in cooperation with traditional actuators in order to meet the vehicle objectives hierarchy. Modern and classical control theory investigate the application of IFAs to control various vehicle output signals.

Keywords: Electrodynamic Actuators, Active Suspensions, Vehicle Dynamics.

1 INTRODUCTION

The primary objectives of vehicle suspensions (passive and active) involve four aspects: suspend the vehicle above the road, maintain relatively constant nominal posture with respect to the road, maintain tractive normal force between the tires and the road, and isolate the vehicle from undesired road-induced vibration (Tseng and Hrovat 2015). Conventional passive suspensions contain hardware traditionally consisting of two devices: a spring element k_s, which generates a force opposing a relative displacement; and a damper element b, which generates a force opposing a relative velocity. Both these elements are outfitted between the wheel (the *unsprung mass*, m_{us}) and the vehicle body (the *sprung mass*, m_s). The tire can also be considered part of the passive suspension, since its representation for vertical dynamics is also a spring, k_t, acting between the unsprung mass and the road. This configuration is represented by a low order model known as a quarter car (QC) (Figure 1).

Although the passive suspension configuration described is convenient for compact packaging, it has drawbacks. Analysis of QC models reveals them as having undesirable resonance in the low frequency passband, as well as undesirable high frequency isolation performance (Karnopp 1983). From the framework of random process theory, it was discovered that optimal frequency response characteristics are achieved when the damper location is moved to between inertial space and the mass for a single degree of freedom (DOF) mechanical resonator (Karnopp, Crosby, and Harwood 1974). This is known as a Skyhook suspension (Figure 2).
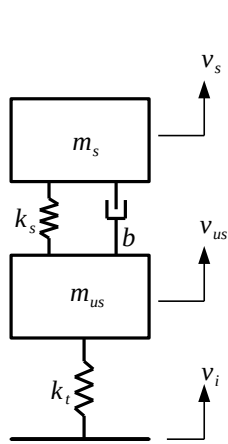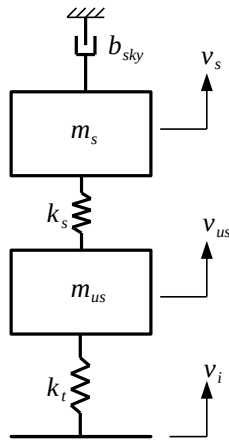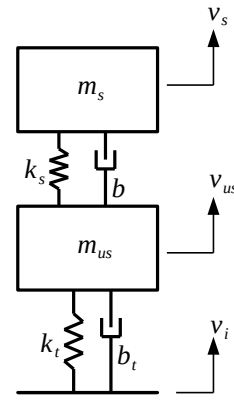
Figure 1: QC model Figure 2: Skyhook QC model Figure 3: Groundhook QC model

When applied to the 2 DOF quarter car, the Skyhook configuration results in better passband performance with a less pronounced 1st resonance peak, and faster isolation roll-off at the cost of an undamped resonance. Figure 4 shows that there is some benefit of maintaining some passive damping between the sprung and unsprung masses in the conventional location, since tire oscillation (2nd resonance) is more damped, although the resulting sprung mass velocity magnitudes are increased in some regions, and high-frequency roll-off benefits of Skyhook are lost. Also, although no physically realizable passive Skyhook suspension for vehicles has been developed, it serves as an optimal structural configuration for model reference of a controlled suspension, and has been the baseline for vehicle active suspensions for several decades.

Lateral and longitudinal vehicle performance is associated with maintaining a near-constant normal force between the tires and the road. This is due to the nonlinear, locally concave constitutive relationship from tire-road normal force to lateral and longitudinal tire force (Karnopp 2013). For this reason, actuators placed in the conventional location (between the unsprung and sprung mass, parallel with the suspension spring and damper) inevitably deteriorate vehicle handling performance. This is a well recognized phenomenon (Smith and Walker 2000) that is a structural limitation of conventional active suspension configurations manifested as an inverse performative relationship between ride comfort and tire dynamic load (which corre-
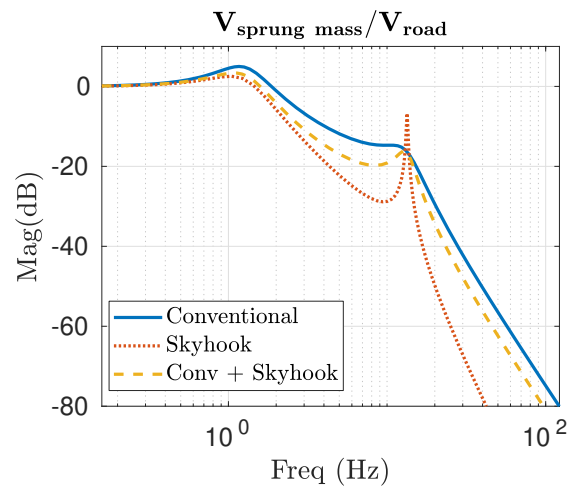

Figure 4: Frequency response of Conventional passive (Figure 1), Skyhook (Figure 2), and Skyhook with an included conventional suspension damper (combination of Figures 1 and 2)

lates with vehicle agility). With respect to performance trade-offs associated with active dampers, it has been observed that the trade-offs could be mitigated if one could exert forces more arbitrarily on a vehicle (Karnopp 1983).

Groundhook (Valášek, Novák, Šika, and Vaculín), inspired by Skyhook, originally sought to minimize damage to roadways from heavy trucks. However, by reducing the dynamic tire force transmitted to the road, Groundhook found benefit for handling performance purposes, since large val-

ues of dynamic tire force also deteriorate road-holding. The Groundhook model (Figure 3) serves as an idealized passive model reference to minimize tire normal force variations due to road-normal velocity inputs, v_i. In reality, the tire damping of Groundhook is difficult to implement with a passive element (Kim, Chi, and Lee 2007). Therefore, like Skyhook, Groundhook is realized through an active- or semi-active suspension designed to track the model reference (MR) containing a virtual damper in series with the tire spring (parameter b_t in Figure 3).

Efforts have been made to mitigate the known performance and handling trade-offs observed in conventional active suspensions. Human comfort from vertical dynamics has highest sensitivity in the 4-8 Hz Frequency band (ISO 2631-1 1997), while tire sensitivity is highest at its resonance, usually around 8-13 Hz. Researchers have tried a frequency-dependent hybrid Skyhook control which seeks to minimize the deterioration at their respective resonant frequencies (Suda, Nakadai, and Nakano 1998). Others applied H_∞ optimal control techniques to a quarter car with a conventional semi-active actuator and compared results to Skyhook control, and found that the high-order H_∞ controller produced could provide a more comfortable ride across a wider band of frequencies (Sammier, Sename, and Dugard 2003). These techniques still result in a performance trade-off, however the designer has more control over the frequency response shape.

Measurements of road elevation profiles indicate that vertical input from the road can be modeled as a white noise stochastic process with a flat power spectral density (PSD) in the velocity (ISO 8608 1995). The vertical velocity PSD is determined by forward vehicle speed and a static road roughness coefficient. The road unevenness enters the vehicle as a disturbance, and degrades both the ride comfort and vehicle handling objectives. However, since physical roadway inputs are well characterized, new vehicle system research is well-suited for simulation studies.

Inertial force actuators (IFAs) (also known as proof mass actuators) have been applied to various vibrations problems. In structural systems, they are used as active force generators to counteract struc-tural resonances where a simple tuned vibration absorber (TVA) would be insufficient, or where the dynamic properties of complex structures are variable (Díaz, Pereira, Hudson, and Reynolds 2012). Other researchers have utilized such actuators for automotive applications to minimize structure-borne acoustic noise (Belgacem, Berry, and Masson 2012) . In another study, IFAs were analyzed for generic structural vibration isolation (Benassi and Elliott 2004). They made the observation that inertial actuators should have a natural frequency that is lower that the natural frequency of the system to be isolated for best performance. The application of an inertial actuator to control vibration of a single-DOF mechanical resonator has also been investigated using velocity feedback (similar to Skyhook) (Elliott, Serrand, and Gardonio 2001). Their main interest was in comparing performance of an inertial actuator to an actuator in parallel with the resonator spring, and identifying conditions under which the controlled system remained stable. Also for vibration isolation of a generic single DOF mechanical resonator, (Zilletti 2016) developed a velocity feedback algorithm that showed reduced vibration of the system. They analyzed the system stability and performance trade-offs, and investigated the conditions under which the inertial actuator would harvest or dissipate power.

Due to the trade-offs between handling and comfort, and the structural limitations of the conventional actuator configuration, this research proposes the application of IFAs for active control of vehicles. In particular, the focus will be on applying these actuators in multi-input, multi-output (MIMO) arrangements with conventional active suspensions. The purpose is to allow for the application of "god" forces onto the vehicle by the reactive force of pushing on the small inertia.

2 A SKYHOOK AND GROUNDHOOK BASELINE ANALYSIS

This research begins with the analysis and implementation of a Skyhook + Groundhook system (the MR) utilizing combined conventional and inertial actuators (the active/actuated system). A schematic of the proposed Skyhook+Groundhook MR is shown in Figure 5. Equations of motion

are derived using this bond graph following procedures of (Karnopp, Margolis, and Rosenberg 2012).
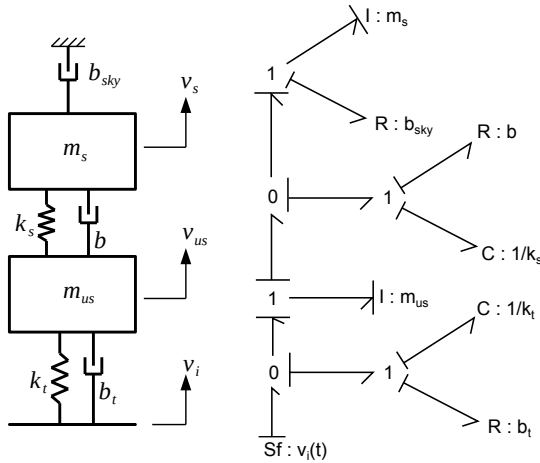

Figure 5: Model reference system and bond graph

From the equations of the MR system, the transfer functions $\frac{v_s}{v_i}\big|_{des}(s)$ and $\frac{v_i - v_{us}}{v_i}\big|_{des}(s)$ are derived, and will be used to generate controllers for the active system. These represent the sprung mass velocity response and the dynamic tire velocity response of the MR.

The actuated system model to be controlled and associated bond graph is shown in Figure 6. Again, equations of motion are generated directly from the causal bond graph.

From the actuated system equations, the transfer functions of Equations 1 are derived. These equations relate the outputs of interest (sprung mass velocity and tire spring velocity) to the controlled inputs (F and F_a) and the disturbance input (v_i). To develop the control, it is recognized that the total responses of the outputs will be a superposition of the inputs multiplied by the respective transfer functions of Equations 1.

$$
\begin{array}{cc}
\dfrac{v_s}{v_i}(s) & \dfrac{v_i - v_{us}}{v_i}(s) \\[2mm]
\dfrac{v_s}{F}(s) & \dfrac{v_i - v_{us}}{F}(s) \qquad (1) \\[2mm]
\dfrac{v_s}{F_a}(s) & \dfrac{v_i - v_{us}}{F_a}(s)
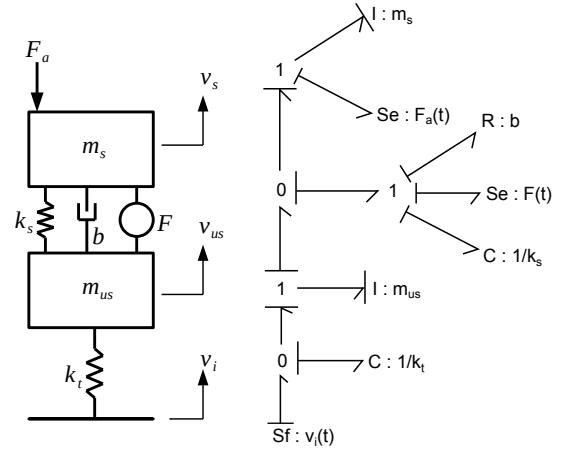\end{array}
$$

Figure 6: Actuated system and bond graph

To make the actuated system follow the idealized MR, we enforce that the actuated system have the same response as the MR:

$$
\begin{aligned}
v_s(s) &= \frac{v_s}{v_i}(s)v_i(s) + \frac{v_s}{F}(s)F(s) + \frac{v_s}{F_a}(s)F_a(s) \\
&= \frac{v_s}{v_i}\bigg|_{des}(s)v_i(s) \\
v_i - v_{us}(s) &= \frac{v_i - v_{us}}{v_i}(s)v_i(s) + \frac{v_i - v_{us}}{F}(s)F(s) \ldots \\
&\quad + \frac{v_i - v_{us}}{F_a}(s)F_a(s) \\
&= \frac{v_i - v_{us}}{v_i}\bigg|_{des}(s)v_i(s)
\end{aligned}
$$

Rearranging these equations into a matrix form allows for the actuator forces transfer function matrix (Equation 2) to be solved by matrix inversion to arrive at the feedforward control on each of the actuators F and F_a that cause the active system to follow the MR system. The actuated quarter car is simulated using parameters of Tables 1 and 2. It should be noted that the only arbitrarily selected parameters for the control are the damping coefficients of the model reference (Table 2). The roadway input v_i is approximately a ISO 8608 Class B road (ISO 8608 1995)(equivalent to the average roadway vehicles encounter (Loprencipe and Zoccali)) with vehicle traveling at 64 kph (40 mph) forward speed. The vertical displacement PSD of the road used for this simulation is shown in Figure 7.

$$\begin{bmatrix} \dfrac{v_s}{F}(s) & \dfrac{v_s}{F_a}(s) \\[2mm] \dfrac{v_i - v_{us}}{F}(s) & \dfrac{v_i - v_{us}}{F_a}(s) \end{bmatrix} \begin{bmatrix} F(s) \\[2mm] F_a(s) \end{bmatrix} = \\[4mm] \begin{bmatrix} \dfrac{v_s}{v_i}\bigg|_{des} & -\dfrac{v_s}{v_i}(s) \\[2mm] \dfrac{v_{us}-v_s}{v_i}\bigg|_{des} & -\dfrac{v_i-v_{us}}{v_i}(s) \end{bmatrix} v_i(s) \tag{2}$$
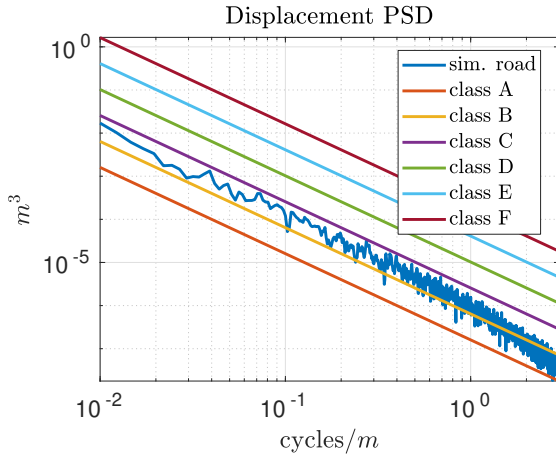
Displacement PSD

Figure 7: PSD comparison between the simulated road and ISO 8608 classes of measured physical roads

Parameter	Value
m_s	312.5 kg
m_{us}	52.5 kg
k_s	20.85 kN/m
b	2042 N m/s
k_t	350.3 kN/m

Table 1: Parameter values for passive elements of quarter car

Parameter	Value
b_t	4084 N m/s
b_{sky}	6126 N m/s

Table 2: Parameters for virtual elements used for control of MIMO Skyhook+Groundhook

Magnitude bode plots of several responses are shown in Figure 9. Several items from these plots can be observed. Primarily, the sprung mass veloc-

ity response is reduced across almost the entire frequency band in the actuated system *without* degradation of tire velocity. Also, the region of highest human sensitivity to vertical acceleration (4-8 Hz, the frequencies between the two resonances) has been reduced.

However, the model and control analysis thus far has depended on several unrealistic assumptions, the most egregious being that the intended inertial force F_a has been perfectly applied to the vehicle with no regard for *how*. Armed with the training provided by bond graphs' port-based approach, we assume an inertial actuator connected to the sprung mass is a simple 1-DOF oscillator in parallel with a force actuator (Figure 8). The bond with effort labeled F_a could be ported into Figure 6 to replace the effort source there labeled F_a.
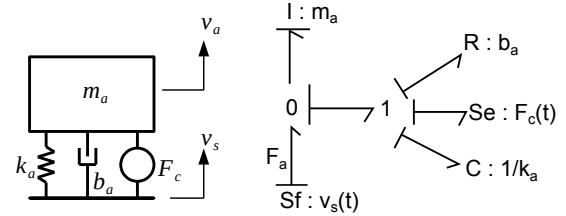

Figure 8: A model of a 1-DOF inertial actuator and its bond graph

Instead of integrating the added dynamics to re-compute the control law of Equation 2 for the new controlled input F_c, we derive the transfer functions from the equations of motion of the 1-DOF, 2nd order, 2-input actuator (Equations 3).

$$\frac{p_a}{v_s}(s) = \frac{b_a s + k_a}{s^2 + \frac{b_a}{m_a}s + \frac{k_a}{m_a}} \qquad \frac{p_a}{F_c}(s) = \frac{s}{s^2 + \frac{b_a}{m_a}s + \frac{k_a}{m_a}}$$

$$\frac{q_a}{v_s}(s) = \frac{s}{s^2 + \frac{b_a}{m_a}s + \frac{k_a}{m_a}} \qquad \frac{q_a}{F_c}(s) = \frac{\frac{1}{m_a}}{s^2 + \frac{b_a}{m_a}s + \frac{k_a}{m_a}}$$

$$\tag{3}$$

The output, F_a, can be calculated by following causality shown in Figure 8. By inspection, we see that $F_a = \frac{dp_a}{dt} = sP_a(s)$. Therefore, from Equations 3 we can derive transfer functions for the output F_a as
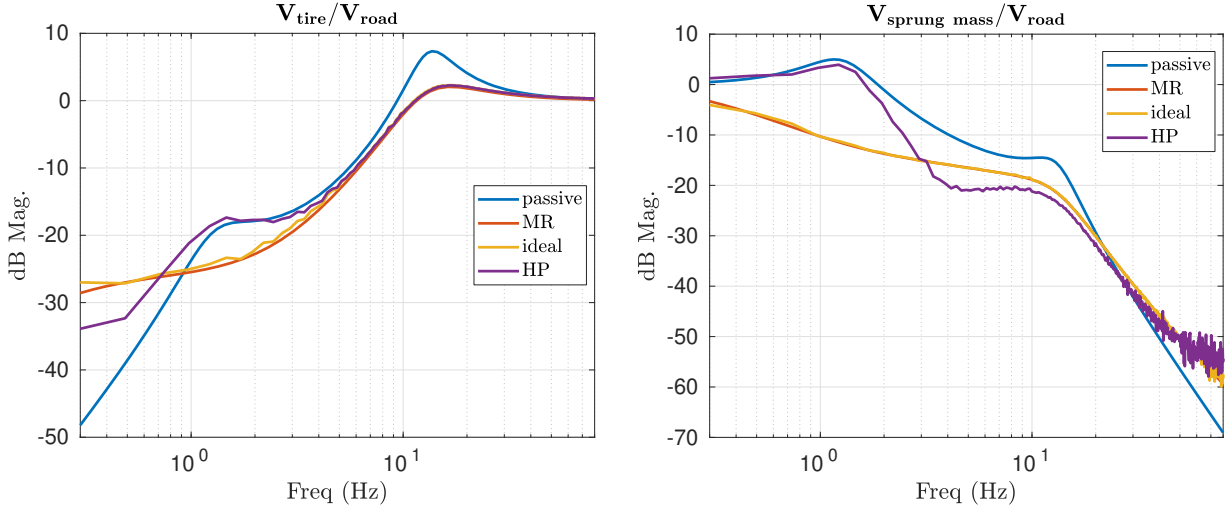
Figure 9: Magnitude frequency response plots (computed from FFT of simulation timeseries unless noted otherwise). Passive: passive system (Figure 1, computed from transfer function). MR: Model reference (Figure 5, computed from transfer function). Ideal: Feed-forward controlled system with inertial force F_a (Figure 6). HP: same as Ideal, but with a high-pass filter applied to F_a.

$$\frac{F_a}{v_s}(s) = \frac{b_a s^2 + k_a s}{s^2 + \frac{b_a}{m_a}s + \frac{k_a}{m_a}} \qquad \frac{F_a}{F_c}(s) = \frac{s^2}{s^2 + \frac{b_a}{m_a}s + \frac{k_a}{m_a}}$$

Again applying principle of superposition we arrive at the total actuator force F_a

$$F_a(s) = \frac{F_a}{v_s}(s)v_s(s) + \frac{F_a}{F_c}(s)F_c(s) \qquad (4)$$

Solving Equation 4 for F_c,

$$F_c(s) = \left(\frac{F_a}{F_c}(s)\right)^{-1}F_a(s) - \frac{F_a}{v_s}(s)\left(\frac{F_a}{F_c}(s)\right)^{-1}v_s(s) \qquad (5)$$

Because the transfer function $\frac{F_a}{F_c}(s)$ is proper, but not strictly proper, the direct inversion is justified. Since we already have the timeseries from the simulation for signals F_a and v_s, we can pass them through their respective 'filters' in Equation 5 to acquire the control signal $F_c(t)$ on the actuator of Figure 8 that imposes the controlled signal F_a from Equation 2 onto the sprung mass.

Next, we can acquire the q_a timeseries, which represents the actuator displacement for the simula-tion.

$$q_a = \frac{q_a}{v_s}v_s + \frac{q_a}{F_c}F_c \qquad (6)$$

Parameters are chosen such that the simple actu-ator has $m_a = \frac{m_s}{100}$, natural frequency of around 1 Hz, and very little damping. Results are shown in Figure 10. The results show that the system and parameters are totally unrealistic for the given inputs.

As a second attempt, we could increase the spring rate to try to keep the actuator displacement near equilibrium, but this would result in F_c needing to fight the spring and damper more often. Since the results of Figure 10 suggest a DC component required by the control, we try passing this signal through a high-pass (HP) filter $\frac{s}{s+w_h}$ before applying it to the actuator. We arbitrarily choose a cutoff w_h of around 2 Hz. Results are shown in Figure 11, and the actuator displacement has been reduced by a factor of 100. The impact of the HP filter on the tire and sprung mass dynamics can be seen in Figure 9, which shows that the system with the HP filter maintains better performance compared to the passive system.

Signal RMS results for the system simulations dis-cussed so far are shown in Table 3. The results sug-
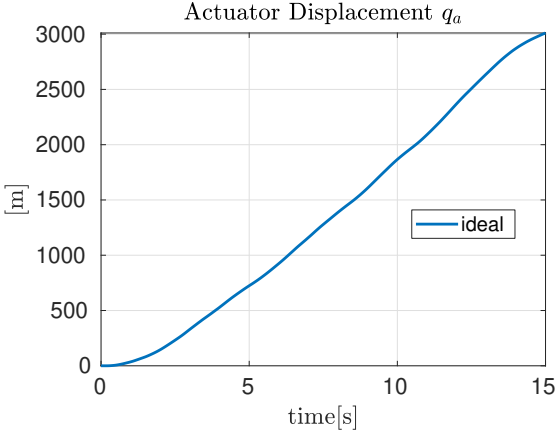
Figure 10: Actuator travel explodes to 3km in one direction, suggesting large DC component to F_a
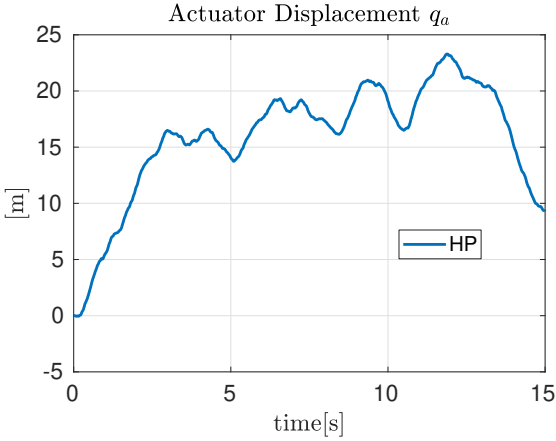

Figure 11: Actuator travel when a high-pass filter is applied to F_a

gest that some benefit may be found in implementing an IFA with a conventional active suspended vehicle, but further adjustments to the control parameters of the system discussed shows diminishing benefit. Therefore, a different approach is tried with optimal control.

3   OPTIMAL CONTROL

In this section, a system analysis utilizing optimal control is presented. We begin by introducing the mechanical 1-DOF, 3rd order multi-energy domain model of Figure 12. This is a simple model of a voice coil actuator, with voltage V and veloc-

	Passive	Ideal	HP
$\dot{\mathbf{v}}_{\mathbf{s}}, \frac{m}{s^2}$	1.17	0.730	0.672
$\mathbf{v}_{\mathbf{s}}, \frac{m}{s}$	0.06262	0.0240	0.0562
$\mathbf{q}_{\mathbf{t}}, m$	0.00200	0.00157	0.00154
$\mathbf{q}_{\mathbf{a}}, m$		1649	16.6
$\mathbf{q}_{\mathbf{s}}, m$	.00622	.00960	.00723
$\mathbf{F}_{\mathbf{a}}, N$		497	452
$\mathbf{F}, N$		380	380

Table 3: Results of simulation using optimal controller (all results are RMS values)

ity v_s inputs and force output F_a. Parameters for this model are chosen from an an off-the-shelf unit (Motran Industries). This actuator is 'ported' in to the vehicle model of Figure 6.
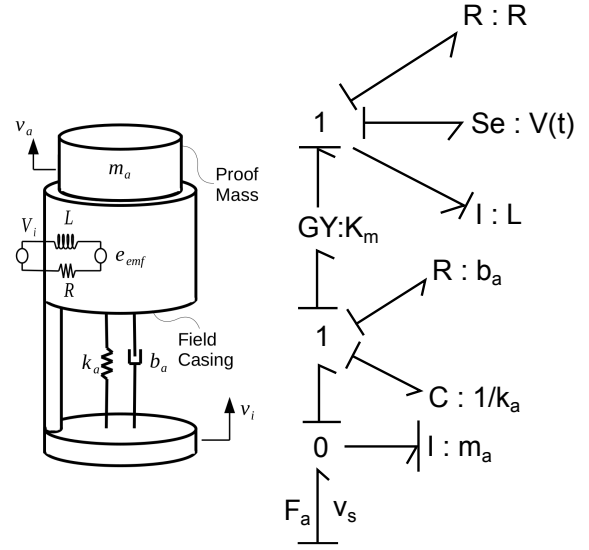

Figure 12: IFA actuator and bond graph for the optimal control analysis

Bond graphs are used to derive the system equations, and from the bond graphs we can see that this is a 7th order system (combined systems of Figures 6 and 12; 4 inertias and 3 capacitances, all in integral causality).

We frame the optimal control problem as an infinite horizon, continuous-time quatradic optimization, also known as a linear quadratic regulator (LQR). First, a cost function is formulated,

$$J = \int_0^\infty \alpha_q q_a^2 + \alpha_a \dot{p}_s^2 + \alpha_t q_t^2 + \alpha_F F^2 + \alpha_V V^2 \ dt \tag{7}$$

where the α_i are tuned parameters whose values are selected to provide desirable results for the system outputs (consisting of system states and state derivatives) and control force signals that we want to minimize. This cost function is converted into standard form by transforming the α_i such that they populate the Q,R, and N matrices of

$$J = \int_0^\infty x^T Q x + u^T R u + 2x^T N u \ dt \tag{8}$$

The cost function minimizer is the state feedback control law

$$u = -Kx \tag{9}$$

with static gain matrix K, where $K = R^{-1}(B^T P + N^T)$ and P is found by solving the Riccati equation

$$A^T P + PA - (PB + N)R^{-1}(B^T P + N^T) + Q = 0$$

The vehicle passive element parameters of Table 1 are again used, and the system is simulated with inputs from the feedback control law of Equation 9 and a disturbance input v_i (an ISO 8608 Class B road (ISO 8608 1995) with vehicle traveling at 64 kph forward speed, which is the same input as in Figure 7). For comparison, a passive quarter car is simulated over the same road input. After some tuning of the α_i cost function parameters of Equation 7, the frequency response plots of Figure 13 were generated.

Figure 13 shows that *both* tire displacement and sprung mass acceleration are reduced across the majority of the frequency band, particularly at the resonances. These results are normally mutually exclusive, exhibiting a waterbed effect on one when the other is optimized in a conventional active suspension (Williams 1997), and suggests efficacy to the proposed IFA as it applies to vehicles.

Some results of interest are in Table 4. The RMS sprung mass acceleration, RMS tire displacement, and RMS actuator displacement are all reduced. It should be noted that the suspension displacement RMS has increased. This is an inevitable byproduct of the chosen cost (Equation 7), and

in the limit of zero sprung mass acceleration and zero tire spring displacement (which is, according to road-holding and comfort, the desired response of the system), the spring displacement has significant dynamic deflection, following the road input exactly. Suspension deflection is an important signal for consideration, and too much could be inadmissible, and future research will investigate constrained optimization and include the suspension deflection to ensure travel limits are accounted for within the controller.

	Passive	LQR
$\dot{\mathbf{v}}_\mathbf{s}, \frac{m}{s^2}$	1.17	.700
$\mathbf{v}_\mathbf{s}, \frac{m}{s}$	0.063	.061
$\mathbf{q_t}, m$	.00200	.00194
$\mathbf{q_a}, m$		.0206
$\mathbf{q_s}, m$	.00622	.02554
$\mathbf{V}, V$		58.7
$\mathbf{F}, N$		549
$\mathbf{Power_V}, W$		187
$\mathbf{Power_F}, W$		97.82

Table 4: Results of simulation using optimal controller (all results are RMS values)

Another item to note is the power requirement of the actuators, which, when compared to the power required to maintain constant velocity of an automobile (60mph is on the order of 10kW (Leung and Williams 2000) (Salihi 1973)), seems acceptable. However, from the viewpoint of the vehicle's power plant, *average* power is a better indicator of energy demand, because unlike the RMS power, average power takes into account power flow direction. Figure 14 shows that the combined actuators' running average power dissipated (equivalent to the integral total power load on the vehicle electrical supply over time) is about 80 Watts. The RMS power of Table 4 should, however, still be used as a guide for actuator sizing.

4 DISCUSSION

The models used for this paper put the actuator directly onto the sprung mass. There are arguments for placing the actuator elsewhere; for instance, it could be placed directly on the unsprung mass. There are important considerations in the
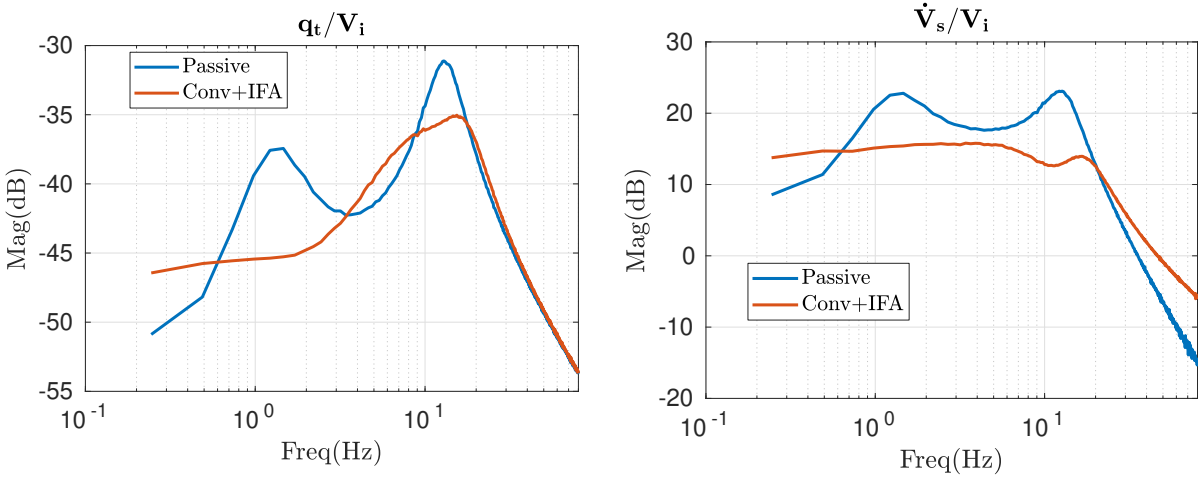
Figure 13: Magnitude frequency response plots of passive system of Figure 1 and active system of Figure 6 with actuator model of Figure 12 to the Class B road input at 64kph.
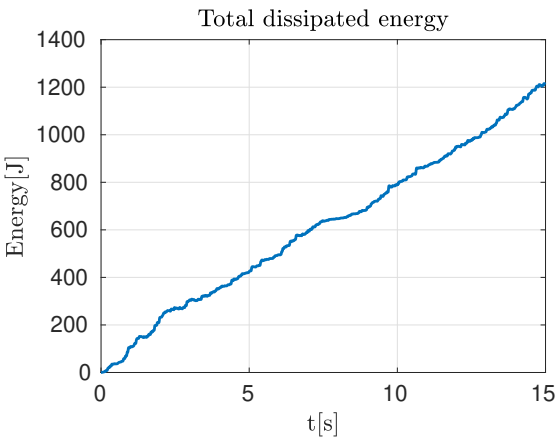
.

Figure 14: Integral of the sum of the instantaneous total power vs time signals of the two actuators

choice of actuator placement. If placed on the unsprung mass, the actuator would be in the best location to filter the disturbance input since there are fewer integrators between the disturbance and the IFA filter. However, the added fixed weight of the actuator housing would decrease the sprung-to-unsprung mass ratio, which has been shown to deteriorate vehicle performance (Hrovat 1988). Alternatively, if the actuator maximum allowable displacement is sufficiently large, the actuator could potentially offset this problem and allow the tire to maintain the desired constant normal force with the ground.

When placed on the sprung mass, the actuator can directly manipulate one of the controlled output variables (sprung mass acceleration), but is several integrators away from the disturbance input. Also, since the sprung mass to proof mass ratio is rather large, significant actuator displacement and/or actuator mass may be needed to operate effectively. These issues, the efficacy of actuator placement, design, and parameters, are points for future research.

The simulated output signals of primary objectives and secondary constraints mentioned or implied (minimal variation of tire displacement from nominal; minimal sprung mass acceleration; minimal displacement of inertial force actuator from nominal; minimal power demand by active suspension system on vehicle power system) favorably suggest that research may be best cast in a constrained optimization framework, and our future research will attempt to consider hard and soft constraints.

5 CONCLUSION

An application of IFAs for active vehicle suspensions has been proposed. The primary goals of this new system are to maximally increase vehicle handling and comfort performance metrics, with the secondary goal of minimal power demand on the vehicle electrical system by the controlled actua-

tors. The proposal is motivated by suggestions in the research that inertial forces on vehicles would garner specific advantages. This proposal emphasizes that these inertial forces can be applied using IFAs, particularly when cast as a MIMO control problem with conventional actuators. Skyhook and Groundhook, and optimal control results were presented. The results of these simulations are promising for further investigation and analysis of the proposed active suspension platform, in part because the MIMO configuration (IFA and conventional suspension actuation) broadens the configuration space of the controlled system.

REFERENCES

Belgacem, W., A. Berry, and P. Masson. 2012, July. "Active vibration control on a quarter-car for cancellation of road noise disturbance". *Journal of Sound and Vibration* vol. 331 (14), pp. 3240–3254.

Benassi, L., and S. Elliott. 2004, December. "Active vibration isolation using an inertial actuator with local displacement feedback control". *Journal of Sound and Vibration* vol. 278 (4-5), pp. 705–724. 00069.

Díaz, I. M., E. Pereira, M. J. Hudson, and P. Reynolds. 2012, August. "Enhancing active vibration control of pedestrian structures using inertial actuators with local feedback control". *Engineering Structures* vol. 41, pp. 157–166. 00042.

Elliott, S. J., M. Serrand, and P. Gardonio. 2001, April. "Feedback Stability Limits for Active Isolation Systems with Reactive and Inertial Actuators". *Journal of Vibration and Acoustics* vol. 123 (2), pp. 250–261. 00137.

Hrovat, D. 1988, August. "Influence of unsprung weight on vehicle ride quality". *Journal of Sound and Vibration* vol. 124 (3), pp. 497–516.

ISO 2631-1 1997. "2631-1: Mechanical vibration and shock-evaluation of human exposure to whole-body vibration-Part 1: General requirements". *Geneva, Switzerland: ISO*. 00331.

ISO 8608 1995. "Mechanical vibration–road surface profiles–reporting of measured data". *International Organization for Standardization, Geneva.*

Karnopp, D. 1983, December. "Active Damping in Road Vehicle Suspension Systems". *Vehicle System Dynamics* vol. 12 (6), pp. 291–311. 00446.

Karnopp, D. 2013. *Vehicle dynamics, stability, and control*. 2nd ed ed. Number 221 in Dekker mechanical engineering. Boca Raton, FL, CRC Press. 00030.

Karnopp, D., M. J. Crosby, and R. A. Harwood. 1974. "Vibration control using semi-active force generators". 01786 ISBN: 0022-0817.

Karnopp, D. C., D. L. Margolis, and R. C. Rosenberg. 2012. *System dynamics: modeling, simulation, and control of mechatronic systems*. John Wiley & Sons.

Kim, B. S., C. H. Chi, and T. K. Lee. 2007, May. "A study on radial directional natural frequency and damping ratio in a vehicle tire". *Applied Acoustics* vol. 68 (5), pp. 538–556.

Leung, D., and D. Williams. 2000. "Modelling of motor vehicle fuel consumption and emissions using a power-based model". In *Urban Air Quality: Measurement, Modelling and Management*, pp. 21–29. Springer.

Loprencipe, G., and P. Zoccali. "Use of generated artificial road profiles in road roughness evaluation". vol. 25 (1), pp. 24–33.

Motran Industries. "IFX400-100 inertial actuator datasheet". http://www.motran.com/inertial-force-actuators.html.

Salihi, J. T. 1973, September. "Energy Requirements for Electric Cars and Their Impact on Electric Power Generation and Distribution Systems". *IEEE Transactions on Industry Applications* vol. IA-9 (5), pp. 516–532.

Sammier, D., O. Sename, and L. Dugard. 2003, April. "Skyhook and H8 Control of Semi-active Suspensions: Some Practical Aspects". *Vehicle System Dynamics* vol. 39 (4), pp. 279–308. 00239.

Smith, M. C., and G. W. Walker. 2000, March. "Performance Limitations and Constraints for Active and Passive Suspensions: a Mechanical

Multi-port Approach". *Vehicle System Dynamics* vol. 33 (3), pp. 137–168. 00074.

Suda, Y., S. Nakadai, and K. Nakano. 1998, January. "Hybrid Suspension System with Skyhook Control and Energy Regeneration (Development of Self-Powered Active Suspension)". *Vehicle System Dynamics* vol. 29 (sup1), pp. 619–634.

Tseng, H. E., and D. Hrovat. 2015, July. "State of the art survey: active and semi-active suspension control". *Vehicle System Dynamics* vol. 53 (7), pp. 1034–1062. 00133.

Valášek, M., M. Novák, Z. Šika, and O. Vaculín. "Extended Ground-Hook - New Concept of Semi-Active Control of Truck's Suspension". vol. 27 (5), pp. 289–303.

Williams, R. A. 1997, June. "Automotive active suspensions Part 1: Basic principles". *Proceedings of the Institution of Mechanical Engineers, Part D: Journal of Automobile Engineering* vol. 211 (6), pp. 415–426. 00214.

Zilletti, M. 2016, May. "Feedback control unit with an inerter proof-mass electrodynamic actuator". *Journal of Sound and Vibration* vol. 369, pp. 16–28. 00033.

AUTHOR BIOGRAPHIES

JORDAN MCCRONE is a graduate student researcher in the Hyundai Center for Excellence at UC Davis, a collaborative venture fostering interaction between students and faculty at UC Davis and engineers from Hyundai in Korea. His research interest is in systems dynamics modeling and control. His email is djmccrone@ucdavis.edu.

DONALD L. MARGOLIS is a professor of mechanical engineering and Director of the Hyundai Center of Excellence at UC Davis. He has extensive experience in teaching system dynamics at the graduate and undergraduate levels, consultation in the vibration control industry, and has published numerous papers on the industrial applications of dynamics. His email is dlmargolis@ucdavis.edu.